Surface spin waves of fcc cobalt films on Cu(100): High-resolution spectra and comparison to theory

J. Rajeswari,[1,3] H. Ibach,[2,3] C. M. Schneider,[1,3] A. T. Costa,[4] D. L. R. Santos,[4] and D. L. Mills[5,*]

[1]*Peter Grünberg Institut (PGI-6), Forschungszentrum Jülich, 52425 Jülich, Germany*

[2]*Peter Grünberg Institut (PGI-3), Forschungszentrum Jülich, 52425 Jülich, Germany*

[3]*Jülich Aachen Research Alliance, Germany*

[4]*Instituto de Física, Universidade Federal Fluminense, 24210-346 Niterói, R. J., Brazil*

[5]*Department of Physics and Astronomy, University of California, Irvine, California 92697, USA*

(Received 12 May 2012; published 22 October 2012)

With the help of a recently developed electron energy-loss spectrometer we have studied the surface spin waves on an eight-monolayer cobalt film deposited on Cu(100) surfaces with unprecedented energy resolution. Standing waves of the bulk of the film are discovered in the region of small wave vectors $q_{\parallel} < 0.35$ Å^{-1}. The dispersion of surface spin waves is isotropic even for large $q_{\parallel}$. Because of the high-energy resolution and the complete characterization of the electron optical properties of the spectrometer reliable data for the linewidth of the surface spin waves are obtained. As a byproduct the dispersion of the Rayleigh surface phonon was measured. Data are compared to theoretical spin wave spectra extracted from calculations of the transverse spin susceptibility based on an *ab initio* electronic structure that incorporates both the metallic substrate and the magnetic film. The calculation takes fully into account the itinerant nature of the electrons responsible for the magnetic moments. The agreement between theoretical and experimental spin wave energies and linewidths is remarkably good.

DOI: 10.1103/PhysRevB.86.165436 PACS number(s): 75.70.Tj, 75.30.Ds

I. INTRODUCTION

The phenomenon of magnetism is characterized by a complex interplay of competing interactions on different length scales. Breaking the inversion symmetry by a surface may cause additional interactions, which eventually determine the magnetic behavior and give rise to new and unexpected effects. Examples are the perpendicular magnetic surface anisotropy which may reorient the magnetization in ultrathin films to point perpendicular to the film plane,[1] ground states with unexpected antiferromagnetic order,[2] or the formation of extended noncollinear spin structures at surfaces in the presence of the Dzyaloshinskii-Moriya interaction.[3] Surface magnetism therefore provides us with a wealth of different magnetic ground states, which depend critically on the details of the system under investigation. While ground states and static properties of many surface and thin-film systems have been investigated in some detail, less is known about their dynamic behavior and the magnetic excitations such as spin waves which, however, may have a profound influence on magnetic ordering and critical phenomena. This is mostly due to the lack of techniques with an appropriate surface sensitivity. Lately, the development of advanced, specifically designed electron energy-loss spectrometers has enabled experimental investigations of surface spin wave excitations in the high-wave vector regime.[4,5] Early studies were made by Vollmer *et al.*[6] with spin-resolved energy-loss spectra of fcc cobalt films deposited on Cu(100). A considerable number of experimental studies on surfaces of cobalt and iron films of varying thickness have appeared since then.[7–11] The issues addressed in these papers concerned primarily the dispersion of surface spin waves, the presence of spin waves in ultrathin films down to one-monolayer thickness,[7,8] and the asymmetry of the spin wave dispersion due to spin-orbit coupling (Dzyaloshinskii-Moriya interaction).[9]

A characteristic feature of the surface spin waves of cobalt and iron is their short lifetime leading to a broad linewidth which increases with increasing wave vector parallel to the surface $q_{\parallel}$. For wave vectors close to the boundary of the surface Brillouin zone the width becomes so large that no clear resonance structure is observed in the energy-loss spectrum.[6] The short lifetime of spin waves is due to the itinerant nature of magnetism in 3*d* transition metals: Spin waves decay rapidly into electron-hole pair excitations involving a spin flip (Stoner excitations). The thereby-caused Landau damping of the spin waves is particularly strong for spin waves in thin films and the surface spin waves of bulk materials since the broken translation symmetry increases the number of available channels for Stoner excitations. Since strong Landau damping leads to a considerable renormalization of the spin wave frequencies Landau damping cannot be considered as a perturbation but is rather to be treated as an integral part of a theoretical description which takes the itinerant nature of 3*d* transition metals into account.[12–15] This entails that for 3*d*-metal films energy and linewidth of spin waves are two sides of the same coin and of equal interest. We note in passing that for nickel surfaces Landau damping is so strong that all attempts to observe surface spin waves in the high wave vector regime have failed although bulk spin waves are clearly observed in neutron scattering.[16]

So far, reliable data on the linewidth of surface spin waves do not exist, not even for cobalt films which provide for the best-defined spin wave signals. An attempt by Etzkorn *et al.* was restricted to the high wave vector regime[17,18] because of the comparatively low-energy resolution of their spectrometer. Based on an estimate of the momentum resolution Etzkorn *et al.* (incorrectly) disregarded the kinematic broadening due to the finite $q_{\parallel}$ range accepted by the energy analyzer. The intrinsic energy width in the medium momentum range was therefore overestimated. As we have shown in a recent technical publication the kinematic broadening can be quite substantial, in particular when the spectrometer operates in a low-resolution mode.[19]

An unresolved puzzle in previous experiments was the absence of any signs of standing wave modes in the spin wave spectra of iron and cobalt films. This is in contrast to observations in inelastic tunneling microscopy on antiferromagnetic Mn layers.[20] Furthermore, models based on local spin torques predict that the number of modes at any surface wave vector matches the number of layers of the magnetic film. Theories which calculate the dynamic magnetic susceptibility for 3*d*-metal films show that for the most part standing spin waves are overdamped so that they lose their character as individual modes. The first standing spin wave at low wave vector, however, should have enough strength and low enough damping to show up in the measured spectra along with the surface spin wave.[14,15,21,22] On the other hand, a recent dynamical analysis of the Heisenberg model showed a complete suppression of standing modes at low wave vectors and at room temperature.[23]

Because of these open questions and contradictions we decided to revisit the issue of surface spin waves in fcc cobalt films deposited on Cu(100). We focus on the eight-monolayer (ML) cobalt film, first, because most of the previous data concern that system; secondly, because the experimental data of Etzkorn *et al.*[7] show that the surface spin wave is practically independent of the number of layers beyond five monolayers. With the help of our recently developed electron spectrometer[5] we obtain spectra of surface spin waves of the 8-ML film as well as standing waves with the unprecedented resolution of 7 meV for wave vectors down to $q_{\parallel} = 0.23$ Å^{-1}. The spectrometer is presently equipped with a standard thermal emission cathode. There are certain disadvantages and advantages associated with the use of an unpolarized source. Disadvantageous is that spin wave signals cannot be separated from vibrational excitations via the spin flip associated with spin wave excitations. This requires very clean surfaces since vibration losses are intrinsically much more intense than spin wave losses. On the other hand, spin waves with arbitrary spin orientation can be studied. We have exploited this feature by studying the spin wave dispersion along the [100] ($\bar{\Gamma}\bar{\mathrm{M}}$) direction in addition to the previously studied spin waves along the easy [110] ($\bar{\Gamma}\bar{\mathrm{X}}$) direction. Our spectrometer is fully characterized with respect to the analyzer acceptance angles.[19] In combination with the spin wave dispersion this permits a quantitative determination of the energy broadening caused by the probed $q_{\parallel}$ range. Quantitative values for the full width at half maximum (FWHM) for the surface spin wave signals are thereby obtained between $q_{\parallel} = 0.23$ Å^{-1} and $q_{\parallel} = 0.9$ Å^{-1}. The high-resolution measurements presented here show evidence of standing wave modes at small $q_{\parallel}$. The results are compared to a completely parameter-free theory of the susceptibility which treats all valence electrons of the system, both at the substrate and at the magnetic film, as itinerant.

The paper is organized as follows: Section II deals with details of the experimental procedures, and a brief description of the spectrometer and the scattering geometry. The high resolution is demonstrated with a spectrum of the surface spin wave of cobalt showing the surface spin wave and the standing wave. Section III presents spectra along both high-symmetry directions for an eight-monolayer film of fcc cobalt on Cu(100). Due to the higher resolution the dispersion of the Rayleigh surface phonon is obtained along with the spin wave dispersion. Section IV is devoted to the analysis of the spectra, in particular to the calculation of the kinematic broadening. The true FWHM of the surface spin wave spectra are thereby obtained. We find that in a wide range of wave vectors the linewidth amounts to about 40% of the spin wave energy. Section V compares the experiment to the results of our theoretical approach in which spin wave spectra are extracted from an *ab initio* calculation of the transverse spin susceptibility.

II. EXPERIMENT

Samples were prepared in an ultrahigh vacuum chamber equipped with facilities for low-energy electron diffraction (LEED), Ar^+ sputtering, Auger electron spectroscopy (AES), medium-energy electron diffraction (MEED), and an evaporator for electron beam stimulated evaporation. Prior to deposition of cobalt the Cu(100) single crystal was cleaned by repeated cycles of Ar^+ sputtering (0.85 keV) and subsequent annealing at 700 K until a sharp well-ordered $p(1 \times 1)$ pattern was observed in LEED. The Co films were deposited at a rate of about 1.25 ML/min from a high-purity rod onto a Cu(100) substrate held at room temperature (RT). During evaporation the base pressure of 1.5×10^{-10} mbar increased to 6×10^{-10} mbar. The Co film grows pseudomorphically on Cu(100) adopting the fcc lattice of the substrate.[24] The thickness of the film was calibrated by monitoring the intensity oscillations of the diffracted beams in a MEED experiment. The oscillations have monolayer periodicity characteristic of layer-by-layer growth.[25] After preparation, the samples were transferred into a separate chamber with base pressure $< 10^{-11}$ mbar housing the electron spectrometer. Small traces of CO detected by their vibration signature in energy-loss spectra were removed from the surface by brief annealing to about 400 K which is below the temperature where interdiffusion of Co and Cu begins (490 K).[26]

The energy-loss experiments are carried out with our high-resolution electron energy-loss spectrometer. The spectrometer features a conventional LaB_6 cathode as electron source and two 143° electrostatic deflectors as monochromators and analyzers each. Furthermore, the spectrometer is equipped with larger slits at the entrance and exit of the deflectors which serves to increase the monochromatic current. High resolution is achieved by the specific design of the second analyzer which reduces the angle aberrations in the plane perpendicular to the dispersion plane (β angles) at the expense of angle aberrations in the dispersion plane (α angles). The larger α angles are then cut off by an angle aperture between the analyzer and detector. This ensures that electrons with large angles with respect to the optical axis after diffuse inelastic scattering from the sample are prevented from entering the analyzer, whereby high resolution is maintained. Furthermore, the spectrometer provides for about five times higher currents than a previous spectrometer designed for studies of spin waves featuring 90°/180° deflectors for monochromatization.[5,27] The high current in combination with the high resolution opens up the possibility to study weak energy losses with high resolution. A detailed description of the spectrometer can be found elsewhere.[5] Because of the conventional cathode, spin

wave excitations can only be identified by their dispersion rather than by spin asymmetry of the scattering as in studies with the 90°/180° spectrometer.[6,11] On the positive side, the use of an unpolarized source enables the investigation of spin waves with arbitrary polarization, a feature that we exploit in our study of the spin wave dispersion along the ⟨011⟩ ($\bar{\Gamma}\bar{\mathrm{M}}$) direction). Also there is no need for orienting the magnetization in the sample. Large wave vector spin waves are strongly damped and travel only about a nanometer, a short distance on the dimensions of spontaneous domains in thin cobalt films.[28]

A schematic representation of the scattering geometry used in the measurements is shown in Fig. 1(a). An incident electron beam at angle $\theta^{(\mathrm{i})}$ referenced to the surface normal with the kinetic energy E_0 and wave vector $\boldsymbol{k}^{(i)}$ is backscattered from the surface. Some electrons undergo inelastic scattering and thereby transfer energy and momentum. The intensity of the scattered electrons with energy E_f and wave vector $\boldsymbol{k}^{(f)}$ is measured at angle $\theta^{(\mathrm{f})}$. Excitations appear as energy losses or energy gains. For elementary excitations characterized by the two-dimensional wave vector $q_\parallel$ and the energy $\hbar\omega$, energy and momentum conservation between the incoming and outgoing electrons requires that

$$E_\mathrm{f} = E_0 \pm \hbar\omega(q_\parallel) \tag{1}$$

and

$$q_\parallel = k^{(\mathrm{f})}\sin(\theta^{(\mathrm{f})}) - k^{(\mathrm{i})}\sin(\theta^{(\mathrm{i})}). \tag{2}$$

In our experiments, the angle between the incoming beam and the scattered beam is kept constant at 90°, which is close to the minimum angle allowed by the spectrometer design. To keep this angle minimal enables the maximum $q_\parallel$ for a given impact energy. The scattering plane is vertical to the surface plane. The required parallel wave vector transfer is achieved by rotating the sample around an axis vertical to the scattering plane. For the impact energies E_0 used here the accuracy in the determination of $q_\parallel$ is 0.004 Å^{-1}.

Depending on the azimuthal orientation of the sample, energies are measured with $q_\parallel$ either along [011] or along [010] corresponding to $\bar{\Gamma}\bar{\mathrm{X}}$ and $\bar{\Gamma}\bar{\mathrm{M}}$ directions in the surface Brillouin zone (SBZ), respectively [Fig. 1(b)]. The SBZ boundary at the $\bar{\mathrm{X}}$ point and the $\bar{\mathrm{M}}$ point is at $q_\mathrm{BZ} = 1.23$ Å^{-1} and $q_\mathrm{BZ} = 1.74$ Å^{-1}, respectively.

Measurements of the dispersion require the accurate knowledge of the kinetic energy E_0 of electrons at the sample. The energy is established in two steps. First, the pass energy E_pass in the monochromator is calculated from the deflection voltage.[5] The kinetic energy is then given by

$$E_0 = E_\mathrm{pass} + e\Delta V + e(\Phi_\mathrm{graphite} - \Phi_\mathrm{sample}), \tag{3}$$

in which ΔV is the voltage difference between the exit of the monochromator and the sample and $e(\Phi_\mathrm{graphite} - \Phi_\mathrm{sample})$ is the work function difference between the graphite-coated exit slit of the monochromator and the sample. The work function difference is experimentally determined by letting the electron beam pass by the sample with the sample surface parallel to the beam while adjusting the sample potential to minimum deflection of the beam.

Our data evaluation procedure is illustrated with the help of Fig. 2. The upper panel of Fig. 2(a) shows a high-resolution spectrum of an eight-monolayer fcc cobalt film on Cu(100)

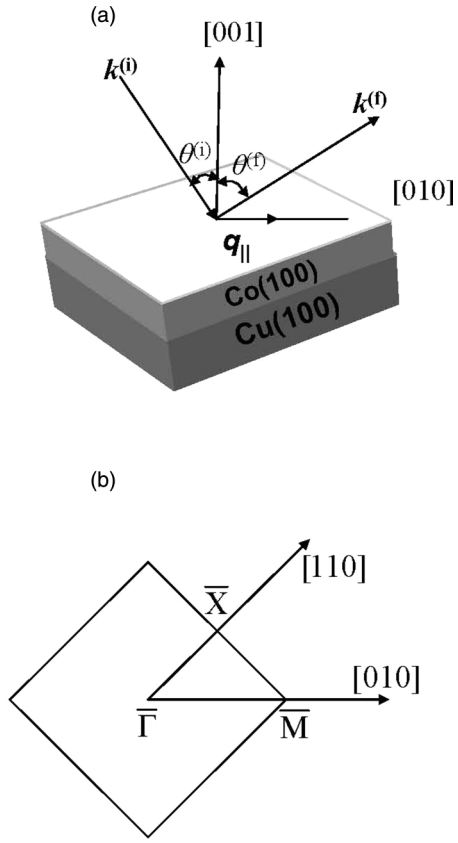

FIG. 1. (a) Schematic illustration of the scattering geometry used in our experiments. For all measurements, the angle between $\boldsymbol{k}^{(\mathrm{i})}$ and $\boldsymbol{k}^{(\mathrm{f})}$, i.e., the scattering angle, is kept constant at 90°.(b) Surface Brillouin zone (SBZ) of the fcc(100) surface with the high-symmetry directions $\bar{\Gamma}\bar{\mathrm{X}}$ and $\bar{\Gamma}\bar{\mathrm{M}}$ indicated.

for $q_\parallel = -0.305$ Å^{-1} along the [011] direction. The incident electron energy is $E_0 = 7.1$ eV. The precise value of the impact energy is not critical. Incident energies between 5.5 and 7.5 eV provide a high cross section for spin wave scattering and high enough momentum to probe wave vectors close to the zone boundary. Energy loss and gain features are assigned to spin wave creation and annihilation, respectively, because of their dispersion with $q_\parallel$ and also by comparison to previous studies using a spin polarized source.[6] The spin wave creation peak (energy loss) at 29.5 meV and annihilation (energy gain) peak at -29.5 meV [marked 1 in Fig. 2(b)] are symmetric with respect to the diffuse elastic peak showing that the frequency of spin waves is independent of the sign of the wave vector as expected for this system[6] (see, however, Ref. 9). Owing to the high resolution and intensity, a second mode at ~ 46.5 meV [marked 2 in Fig. 2(b)] is clearly visible. The second mode is not resolved on the energy-gain side since the probability of having thermally excited spin waves is given by the Bose occupation number $n(\hbar\omega, T)$ which is small (0.17) for a 46-meV energy loss at room temperature. The intensity on the energy-loss side is proportional to $n(\hbar\omega, T) + 1$.[29] Because of this energy-dependent weighting, peak 1 appears larger than it is in relation to peak 2. For the comparison of the intensity and shape of the spin wave signals to theory, the spectrum in Fig. 2(b) is divided by $n(\hbar\omega, T)$ and $n(\hbar\omega, T) + 1$ on the

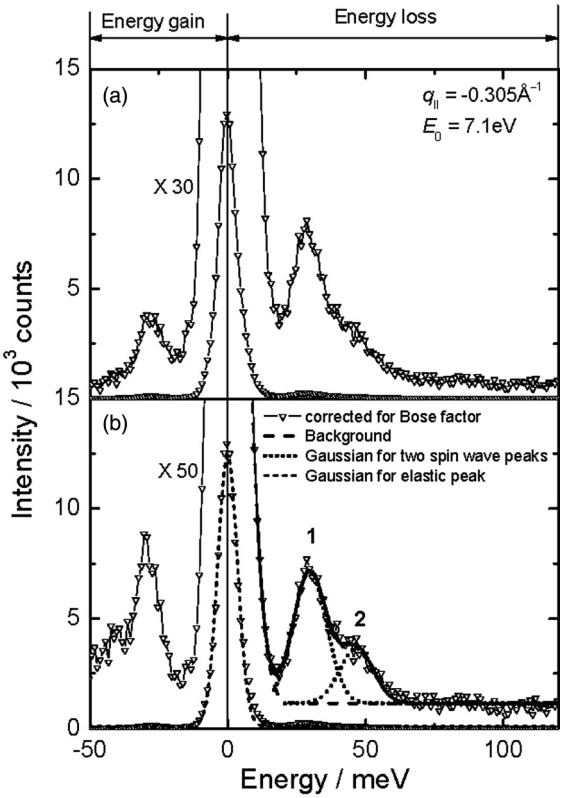

FIG. 2. (a) Spin wave spectrum measured for 8-ML Co deposited on Cu(100) for in-plane wave vector transfer $q_{\|} = -0.305$ Å^{-1} along [011] direction. The primary beam energy is $E_0 = 7.1$ eV. Loss and gain peaks correspond to creation and annihilation of spin waves. (b) Data as in (a), however, divided by the Bose occupation number $n(\hbar\omega,T)$ on the gain side and by $n(\hbar\omega,T)+1$ on the loss side. Spin wave losses 1 and 2 are fitted by Gaussians (dotted line) after subtraction of a Gaussian for the tail of the elastic line and constant background (dashed line).

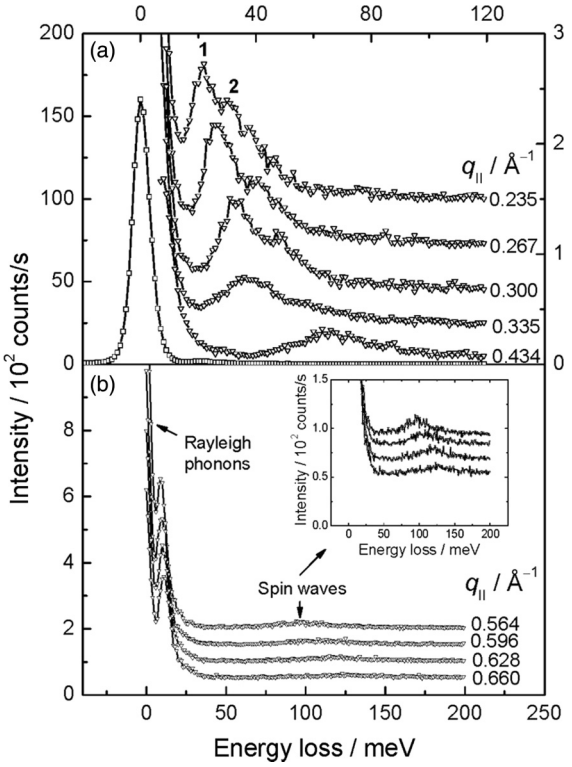

FIG. 3. (a) Series of spin wave spectra measured along [011] direction with high resolution. Spectra are corrected for the Bose occupation number. Two modes of spin waves are clearly visible for low $q_{\|}$. (b) A selection of spectra for larger $q_{\|}$ obtained with the same spectrometer setting. The Rayleigh phonons and spin waves are clearly distinguished. The incident beam energy in all cases is 7.1 eV.

gain and loss side, respectively. The energy, intensity, and eventually the width of the spin wave peaks (Sec. IV) are then determined by fitting the loss side of the spectrum to one or two Gaussians [dotted lines in Fig. 2(b)] after subtraction of a Gaussian background tail of the elastic peak and a constant [dashed line in Fig. 2(b)]. The solid line represents the complete fitting function consisting of the background and the two Gaussians for the spin wave peaks. The diffuse elastic peak is also fitted by a Gaussian (short dashed line) to serve as reference for energy resolution.

III. RESULTS

A series of high-resolution spectra for wave vectors in [011] ($\bar{\Gamma}\bar{X}$) direction ranging from $q_{\|} = 0.235$ to 0.434 Å^{-1} is shown in Fig. 3(a). The FWHM of the diffuse elastic peak is about 7 meV. The primary electron energy is $E_0 = 7.1$ eV. The spin wave peaks are clearly seen as separate peaks down to $q_{\|} = 0.235$ Å^{-1} corresponding to a spin wave energy of about 20 meV. The spectra are measured with gate times of 2–6 s in 1-meV intervals. For smaller wave vectors (<0.3 Å^{-1}), one sees a distinct peak with a shoulder on the high-energy side. The distinct peak is the surface spin wave. As discussed in Sec. V theory identifies the second peak as a standing spin wave mode of the film.

Spectra measured under the same conditions, yet for larger $q_{\|}$, are displayed in Fig. 3(b). The spin wave signals are rather weak now but clearly discernible in higher magnification (see inset). Strong loss features appear at low energies. These energy losses are due to the excitation of Rayleigh phonons (surface acoustic phonons polarized in the sagittal plane).[30] The relatively low energies of Rayleigh phonons (compared to spin waves) combined with the energy resolution of 7 meV used in the experiments allowed for unambiguous distinction between Rayleigh phonons and spin waves.

As seen in Fig. 3(b) the intensities of the spin wave losses are rather low for larger $q_{\|}$. This is partly due to the fact that the spin wave features become broad. For larger wave vectors between 0.4 and 1.0 Å^{-1} we have therefore performed a series of experiments with lower energy resolution. The typical FWHM of the diffuse elastic peak for this set is about 34 meV. The spectra were recorded along the $\bar{\Gamma}\bar{X}$ and the $\bar{\Gamma}\bar{M}$ direction of the SBZ [Fig. 1(b)]. Because of the higher intensities, gate times of 1 s were used for smaller $q_{\|}$ and 2 s for $q_{\|} > 0.85$Å^{-1}. The measurements were performed for both positive and negative wave vector transfers.

Figure 4(a) shows a selection of spin wave spectra measured along the [011] ($\bar{\Gamma}\bar{X}$) direction, and Fig. 4(b) along the [010] ($\bar{\Gamma}\bar{M}$) direction for positive wave vector transfers. The dashed line is a guide to the eye connecting the maxima of the loss

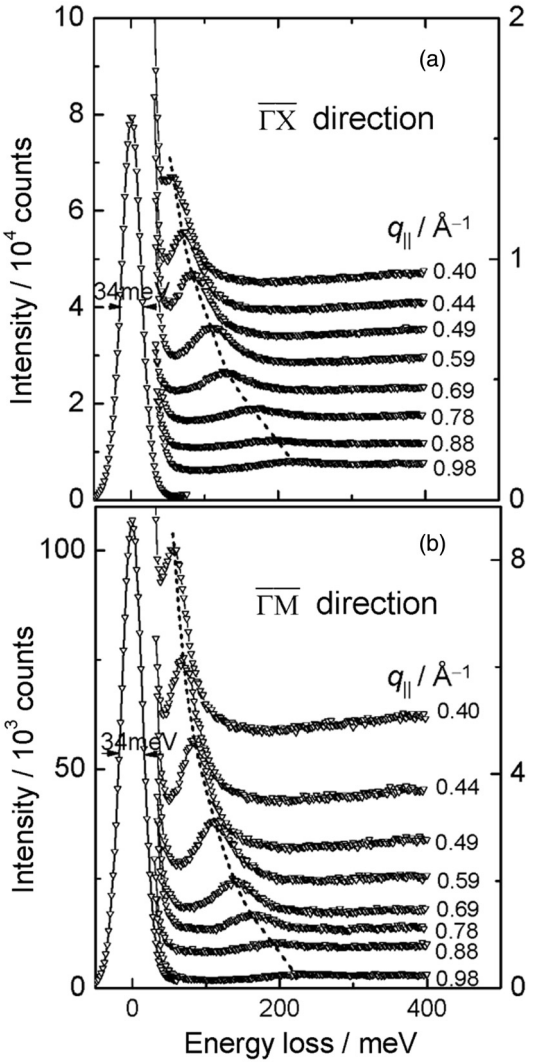

FIG. 4. Series of surface spin wave spectra from an 8-ML cobalt film deposited on a Cu(100) surface for wave vector transfers along (a) [011] direction and (b) along [010] direction. The spectra are offset with respect to each other along the vertical axis. The impact energy on the sample is $E_0 = 7$ eV. The FWHM of the elastic diffuse line is about 34 meV.

peaks. As noted before, the spin wave signal reduces at higher wave vectors and also broadens severely.[6] This is due to the increased coupling of spin waves to Stoner excitations at higher wave vectors which imposes a strong damping (Landau damping) on the spin waves.[22] Owing to this broadening it becomes increasingly difficult to distinguish between spin wave and Stoner excitations beyond $q_{||} = 1.0$ Å^{-1} (see also Ref. 14). It is furthermore difficult to mark definitively the maximum of the spin wave energy loss.

As an example Fig. 5 shows a spectrum for $q_{||} = 1.1$ Å^{-1} measured along the [011] direction: The sharp spin wave energy loss has deteriorated into a broad structure which is not clearly distinct from a continuum of electron-hole pair excitations.

The dispersion of surface spin waves, of the standing waves, and of the Rayleigh phonons along the [011] direction is shown in Fig. 6. The open circles and triangles represent the data

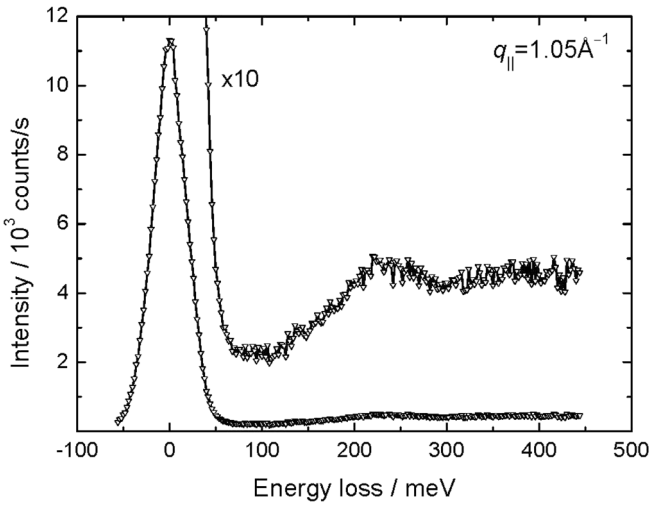

FIG. 5. Spin wave spectrum for $q_{||} = 1.1$ Å^{-1} measured along [011] direction. The spectrum is very broad bringing about a considerable arbitrariness in the determination of a "peak position."

points for the surface spin waves measured with high resolution (7.3 meV) and low resolution (34 meV), respectively. Data points are established following the procedures described in Sec. II. In the overlapping range the data agree well with each other. The peak positions of the standing waves (open squares in Fig. 6) are determined by fitting two Gaussians as illustrated in Fig. 2(b). The thereby-obtained values for the position of the second peak depend significantly on the assumed width of the standing wave peak. We have therefore added error bars for an estimate of the uncertainty in the peak position.

The energies of the Rayleigh phonon are determined by fitting energy loss, energy gain, and the diffuse elastic peak to

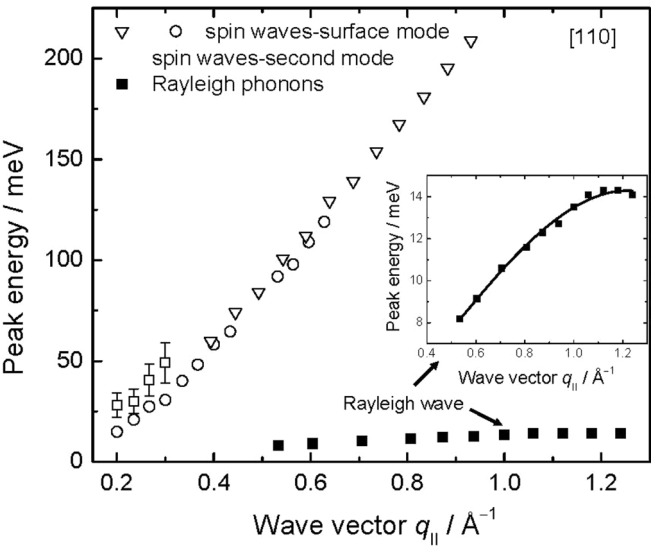

FIG. 6. Dispersion of surface spin waves (open circles and triangles), of the second spin wave mode (open squares) and of the Rayleigh phonon (solid squares) along [011] direction for 8-ML fcc Co/Cu(100) system. The data points marked as circles and squares are obtained from high-resolution spectra (FWHM = 7 meV) whereas the triangles are obtained from low-resolution spectra (FWHM = 35 meV).

three (overlapping) Gaussians. This procedure is justified since phonon creation and annihilation peaks necessarily appear at the same energy because of time reversal symmetry. The Rayleigh phonon dispersion (marked by solid squares in Fig. 6) shows a linear rise for small wave vectors, but becomes, however, flat or even bends downwards near the zone boundary. Our data are roughly consistent with Mohamed *et al.*[31] The downwards bending was noticed for thin Fe films deposited on Cu(100) and interpreted as a signature of compressive surface stress induced by the lattice mismatch between the fcc Fe film and the substrate.[32] However, this interpretation cannot apply to the case of cobalt on copper since the lattice mismatch between fcc cobalt [$a_0 = 3.54$ Å (Ref. 33)] and copper ($a_0 = 3.615$ Å) calls for tensile rather than compressive stress in the cobalt film which should shift the frequency upwards. Since the Rayleigh phonon disperses linearly with $q_\parallel$ at small wave vectors while the spin wave energy scales with $q_\parallel^2$ there must be a crossover. Unfortunately, the crossover is at about $q_\parallel = 0.043\text{Å}^{-1}$ and at an energy of 0.5 meV, far too low to be observable in energy-loss spectroscopy.

The complete spin wave dispersion with data points for positive and negative wave vectors and for $\bar{\Gamma}\bar{X}$ direction (squares and triangles) and $\bar{\Gamma}\bar{M}$ direction (circles) is depicted in Fig. 7. For $\bar{\Gamma}\bar{X}$ the data agree with those reported in the work of Vollmer *et al.*[6] In the limit of small $q_\parallel$, the spin wave dispersion is given by $\hbar\omega = Dq_\parallel^2$ where D is the exchange stiffness of the film. By applying this relation to our data for low wave vector spin waves measured along the [011] direction (solid line), we obtain the value of D as 346 ± 14 meV Å^2. Available Brillouin light scattering (BLS) measurements on a bulk spin wave yields a value of $D = 466 \pm 16$ meV Å^2 as the exchange stiffness for ~1000-Å-thick epitaxial Co films on Cu(100).[34] The lower value of D in our measurements is roughly consistent with the number of nearest neighbors at the surface (eight as opposed to 12). Owing to the fourfold

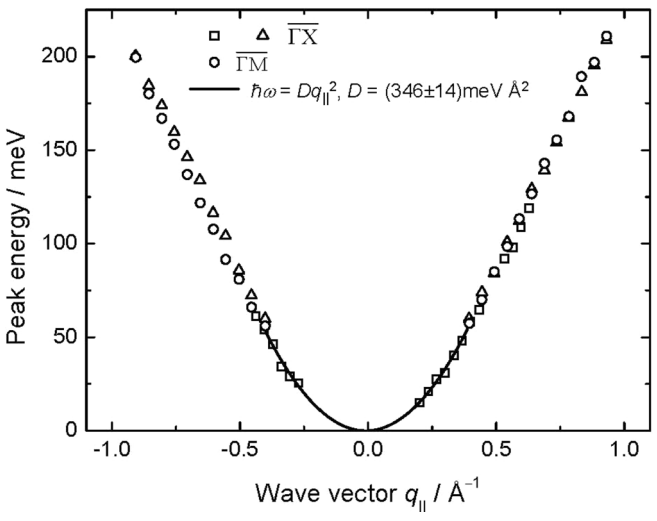

FIG. 7. Dispersion of the spin wave: Squares and triangles represent the dispersion measured with $q_\parallel$ along $\bar{\Gamma}\bar{X}$ while circles mark dispersion along $\bar{\Gamma}\bar{M}$. High-resolution data for small wave vector are fitted with a parabolic dispersion relation, $\hbar\omega = Dq_\parallel^2$ with $D \approx 346$ meV Å^2. Within the limits of accuracy the dispersion is isotropic in the entire range.

symmetry and the quadratic dependence of the frequency on $q_\parallel$ the dispersion is necessarily isotropic at small $q_\parallel$. As seen from Fig. 7, the dispersion remains isotropic even in the limit of large wave vectors as long as a unique peak position can be safely assigned to a spin wave loss.

IV. ANALYSIS OF THE WIDTH OF THE LOSS PEAKS

Figure 3 shows that spin wave energy loss becomes broader the larger its wave vector $q_\parallel$ is. A quantitative study of the width first requires the subtraction of the broadening due to the finite energy resolution. This correction is straightforward as the energy resolution function is provided by the elastic diffuse line in each spectrum [Fig. 2(b)]. In addition one has to take into account that the spectrometer inevitably samples spin wave signals within a finite range of angles α in the scattering plane, equivalent to a range of wave vectors $q_\parallel$. By virtue of the slope of the dispersion curve $d\hbar\omega/dq_\parallel$ the finite range of $q_\parallel$ vectors transforms into a width on the energy scale (kinematic energy broadening). This effect has been discussed earlier by Etzkorn.[18] Based on the measurement of the elastic intensity vs angle Etzkorn concluded that the effect of kinematic broadening was negligible. Our electron optical calculations show that the range of accepted α angles cannot be determined this way.[19] The reason is that the image of the exit slit of the monochromator moves away from the center of the entrance slit of the analyzer upon rotation of the spectrometer angle. Using trajectory calculations of bundles of electrons leaving the monochromator that are scattered diffusely from the sample and enter the analyzer within the angle range accepted by the analyzer we can determine the acceptance angle for diffuse scattering at the sample for any set of voltages applied to the spectrometer lenses.[19] Thereby we can calculate the contribution of the scattering kinematics to the energy width in a spectrum. To the best of our knowledge this aspect has not been covered in previous literature on energy-loss spectroscopy. We therefore briefly attend to this issue in the following.

We first consider the scattering kinematics. For simplicity we assume that the energy loss $\hbar\omega$ is small compared to the impact energy E_0. The wave vector $q_\parallel$ is

$$q_\parallel = \sqrt{2mE_0/\hbar^2}\{\sin\theta^{(f)} - \sin\theta^{(i)}\}, \tag{4}$$

where $\theta^{(i)}$ and $\theta^{(f)}$ are the angles of the electron with respect to the surface normal before and after scattering from the surface and m and E_0 are electron mass and energy, respectively. We consider the case where $q_\parallel$ is chosen by rotating the crystal by the amount $\Delta\theta$ while the mean angle between the incoming and scattered beam remains at 90°.

$$\begin{aligned} q_\parallel &= \sqrt{2mE_0/\hbar^2}\{\sin(45^\circ + \Delta\theta) - \sin(45^\circ - \Delta\theta)\} \\ &= \sqrt{4mE_0/\hbar^2}\sin\Delta\theta \equiv \kappa\sin\Delta\theta. \end{aligned} \tag{5}$$

If the trajectory of the emerging electron makes an angle α with the nominal angle $\theta^{(f)} = 45^\circ + \Delta\theta$ and if this electron is accepted by the lens/analyzer combination then the wave vector transfer for that electron is

$$q_\parallel(\alpha) = \tfrac{1}{2}\kappa\{\sin(45^\circ + \Delta\theta + \alpha) - \sin(45^\circ - \Delta\theta)\}. \tag{6}$$

In agreement with the central limit theorem[35] we find that the angle distribution of diffuse scattering that is accepted by the analyzer is a Gaussian:

$$P(\alpha) = \exp\left[-\alpha^2/2s_\alpha^2\right]. \tag{7}$$

For simplicity we assume that the natural width of the spin wave energy loss for a fixed $q_\parallel$ is also a Gaussian (see also fitting procedures shown in Fig. 3):

$$I(\omega) = I_0 \exp\left\{-[\omega - \omega(q_\parallel)]^2/(2s_\omega^2)\right\}. \tag{8}$$

The intensity response function is therefore

$$R(\omega) = \int_{-\infty}^{+\infty} \exp\left\{-\frac{[\omega - \omega(q_\parallel(\alpha))]^2}{2s_\omega^2}\right\} \exp\left\{-\frac{\alpha^2}{2s_\alpha^2}\right\} \mathrm{d}\alpha. \tag{9}$$

As only small angles α contribute we can expand $\omega(q_\parallel)$ as

$$\omega(q_\parallel) = \omega(q_\parallel(\alpha = 0)) + \left.\frac{\partial\omega}{\partial\alpha}\right|_{\alpha=0} \alpha \equiv \omega_0 + c\alpha. \tag{10}$$

With the latter shorthand notation the response function becomes

$$R(\omega) = \exp\left\{-\frac{(\omega-\omega_0)^2}{2s_\omega^2}\right\} \int_{-\infty}^{+\infty} \exp\left\{-\frac{c^2\alpha^2 - 2(\omega-\omega_0)c\alpha}{2s_\omega^2}\right\} \exp\left\{-\frac{\alpha^2}{2s_\alpha^2}\right\} d\alpha. \tag{11}$$

The integral can be expressed in closed form to yield

$$\int_{-\infty}^{+\infty} \exp\left\{-\frac{c^2\alpha^2 - 2(\omega-\omega_0)c\alpha}{2s_\omega^2}\right\} \exp\left\{-\frac{\alpha^2}{2s_\alpha^2}\right\} \mathrm{d}\alpha \propto \exp\left\{\frac{(\omega-\omega_0)^2}{2s_1^2}\right\} \quad \text{with} \quad s_1^2 = s_\omega^2\left(1 + \frac{s_\omega^2}{c^2 s_\alpha^2}\right). \tag{12}$$

The final response function is then simply

$$R(\omega) \propto \exp\left\{-\frac{(\omega-\omega_0)^2}{2s^2}\right\} \quad \text{with} \quad s^2 = s_\omega^2 + c^2 s_\alpha^2 \equiv s_\omega^2 + \left(\left.\frac{\partial\omega}{\partial\alpha}\right|_{\alpha=0}\right)^2 s_\alpha^2. \tag{13}$$

The derivative of ω with respect to α is split up into the part that comes from the dispersion and the part that comes from the dependence of $q_\parallel$ on α:

$$\frac{\partial\omega}{\partial\alpha} = \frac{\partial\omega}{\partial q_\parallel}\frac{\partial q_\parallel}{\partial\alpha} = \frac{\partial\omega}{\partial q_\parallel}\left\{\frac{1}{2}(q_\parallel - \sqrt{\kappa^2 - q_\parallel^2})\right\}, \tag{14}$$

where $\partial q_\parallel/\partial\alpha$ is obtained from Eq. (6).

To apply this to the case of spin waves of cobalt films we parametrize the dispersion as

$$\hbar\omega = 120\,\mathrm{meV}[1 - \cos(\pi q_\parallel/q_{\mathrm{BZ}})], \tag{15}$$

in which q_{BZ} is the q vector at the boundary of the surface Brillouin zone. Hence $\partial\hbar\omega/\partial q_\parallel$ is

$$\frac{\partial\hbar\omega}{\partial q_\parallel} = 120\,\mathrm{meV}\ \ \pi/q_{\mathrm{BZ}}\sin(\pi q_\parallel/q_{\mathrm{BZ}}). \tag{16}$$

Figure 8 shows the calculated FWHM of spectra resulting from the dispersion and the finite $q_\parallel$ range that is probed by the spectrometer for the s_α calculated for the spectrometer voltage settings used for the spectra shown in Fig. 3 ($s_\alpha = 0.015$) and Fig. 4 ($s_\alpha = 0.045$). Quite remarkably, the FWHM is asymmetric in $q_\parallel$. Best resolution is therefore obtained for positive $q_\parallel$!

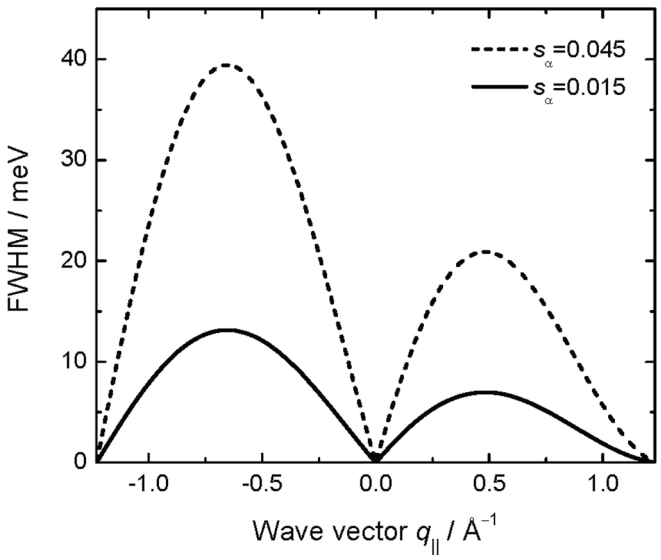

FIG. 8. Calculated kinematic broadening of the spin wave energy-loss peak for two different ranges of acceptance angles α characterized by the Gaussian variance parameters $s_\alpha = 0.045$ and 0.015. The s_α values correspond to FWHM of the angle distribution of 6° and 2°, respectively. Note the asymmetry of the broadening.

Figure 9 shows the FWHM of the experimental spin wave spectra obtained by fitting a Gaussian to the raw data (open circles). Up to $q_\parallel = 0.66$ Å^{-1} corresponding to a spin wave

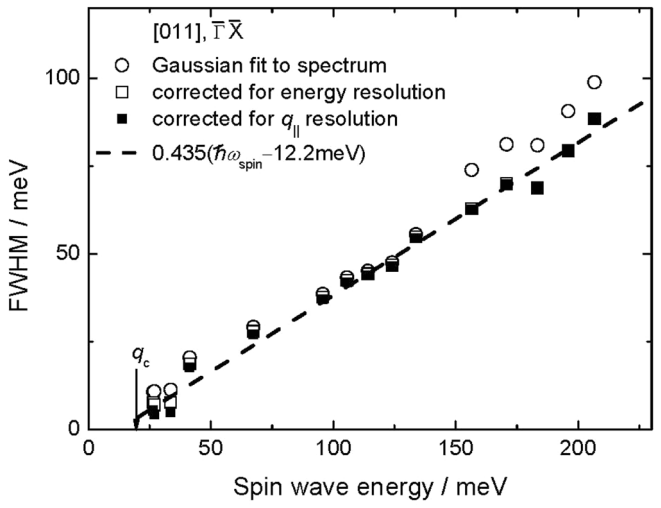

FIG. 9. Determination of the true FWHM of the spin wave peak from experimental spectra. Up to $q_\parallel = 0.66$ Å^{-1} ($\hbar\omega$∼130 meV) experimental spectra have been obtained with an energy resolution of 7 meV FWHM. The variance of the distribution of accepted angles was $s_\alpha = 0.015$. For larger $q_\parallel$, the energy resolution was 34 meV and $s_\alpha = 0.045$. The circles give the experimental FWHM. The open squares represent the values after correction for the energy resolution. The solid squares are obtained after the additional correction for the kinematic broadening. The data are plotted versus the spin wave energy. The dashed line is a linear fit to be discussed later.

energy of $\hbar\omega \sim 130$ meV, the data refer to spectra obtained with an energy resolution of 7.3 meV FWHM (Fig. 3). The variance of the distribution of accepted angles is calculated to $s_\alpha = 0.015$ in that case. For the larger $q_\parallel$, the energy resolution was 34 meV (Fig. 4) and s_α is obtained as $s_\alpha = 0.045$. Since the energy resolution function as given by the elastic diffuse peak (Figs. 3 and 4) is also a Gaussian the resolution-corrected FWHM $\Delta E_{\rm corr}$ is calculated as

$$\Delta E_{\rm corr} = \sqrt{\Delta E_{\rm loss}^2 - \Delta E_{\rm el}^2}, \tag{17}$$

in which $\Delta E_{\rm loss}$ and $\Delta E_{\rm el}$ are the FWHM of the spin wave energy loss and the FWHM of the elastic diffuse line, respectively. The FWHM after correction for the energy resolution are shown as open squares in Fig. 9. The solid squares in Fig. 9 are obtained after the additional correction for the kinematic broadening following Eqs. (13) and (14).

We see that the correction due to the kinematic broadening is relatively small in our case. If however we had probed the lower $q_\parallel$ range with the resolution and the lens settings used for the higher $q_\parallel$ range then the kinematic correction would have been quite substantial (compare Fig. 8). This presumably is the reason why our FWHM obtained in the low $q_\parallel$ range are smaller than reported in the work of Etzkorn.[18] Etzkorn (using the same scattering geometry as ours) also noted a much higher energy width of the spectra for negative $q_\parallel$ which we attribute to the asymmetry that is characteristic of kinematic energy broadening (Fig. 8).

V. THEORY

We now turn to a discussion of the theory of spin waves in the metallic system 8-MLCo/Cu(100). It is by now understood that a correct theoretical description of spin excitations in metallic systems demands taking into account the itinerant character of the electrons responsible for the existence of magnetic moments.[36] In such systems spin waves are strongly damped for all but the smallest wave vectors (see Figs. 4 and 5). At large wave vectors only a very broad structure is seen, in complete (qualitative and quantitative) disagreement with the predictions based on localized spins models. In our theoretical approach all valence electrons of the system, both at the substrate and at the magnetic film, are treated as itinerant. We employ a multiorbital tight-binding Hamiltonian with hopping integrals extracted from DFT-based calculations. This description provides a ground state in good quantitative agreement with various *ab initio* calculations. Magnetism is driven by a screened Coulomb interaction within the d orbitals of the magnetic sites, represented by a multiorbital version of the Hubbard term. The strength of the effective Coulomb interaction is also extracted from the same DFT calculation that provides the hopping parameters.[36] Previous calculations based on the same approach[14,15] showed a good qualitative agreement with experiment. A better quantitative agreement was precluded by the fact that the hopping integrals we employed were not appropriate for the layered structure in question. In fact, they were bulk hopping parameters slightly adapted to the film geometry. We have shown recently, for a different system, that the use of hopping parameters derived specifically for the geometry in question is essential for a good quantitative description of the excitation energies.[37]

For the present calculations we employed tight-binding parameters extracted from a real space linear muffin-tin orbital calculation implemented within the atomic sphere approximation (RS-LMTO-ASA).[38,39] The basic eigenvalue problem is solved in real space using the Haydock recursion method.[39] The 8-ML Co film on the Cu substrate was simulated using a cluster of approximately 9000 atoms, arranged in 13 layers parallel to the (001) surface. One empty-sphere overlayer is included and self-consistent potential parameters were obtained for the empty-sphere overlayer, the 8-ML Co film and three Cu layers underneath using the local spin-density approximation (LSDA).[40] For deeper Cu layers we use bulk potentials. Nine orbitals per site (the five $3d$ and four sp complexes) were used to describe all the atoms in the cluster, including the empty-sphere overlayer.

We obtain spin excitation spectra from the transverse spin susceptibility defined as

$$\chi^{+-}(\omega; \vec{R}_l - \vec{R}_{l'}) = \int dt e^{i\omega t}\{-i\Theta(t)\langle[S^+(t;\vec{R}_l), S^-(0;\vec{R}_{l'})]\rangle\}, \tag{18}$$

where the angular brackets denote thermal average, $S_l^+(t;\vec{R}_l)$ is the spin raising operator in the Heisenberg representation at time t and site $\vec{R}_l$, and $\Theta(t)$ is the Heaviside step function. For systems characterized by a layered geometry, such as the films we are investigating, the translational symmetry in the direction parallel to the layers allows the use of a mixed Bloch-layer representation defined by the transformation

$$|\vec{q}_\parallel, l\rangle = \frac{1}{\sqrt{N_\parallel}} \sum_{\vec{R}_\parallel} e^{i\vec{q}_\parallel \cdot \vec{R}_\parallel} |\vec{R}_\parallel, l\rangle, \tag{19}$$

where $\vec{q}_\parallel$ and $\vec{R}_\parallel$ are a wave vector and a lattice vector parallel to the atomic layers, respectively, and l is a discrete index labeling atomic layers. In this representation the transverse susceptibility becomes a matrix in atomic layer indices and a function of frequency and wave vector parallel to the atomic layers.

We first present the energy dispersion of our calculated spin waves as a function of wave vector along [110] in Fig. 10. The spin wave energies are extracted from our calculations in the same way as they are extracted from experimental data: We identify the peaks of the spectral density with spin wave modes. The energies at which these peaks occur for each value of wave vector form the spin wave dispersion relation. Comparison with the experimental results shows a good agreement for smaller and medium wave vectors. The stiffness obtained from a parabola fit to the low wave vector energies is 400 meV, 12% higher than the experimental result. For higher wave vectors the theoretical data digress from experiment. We speculate that this discrepancy at higher wave vectors comes from the sensitivity of the spin wave dispersion relation to fine details of the electronic structure. The exchange stiffness (that determines the small wave vector spin wave energies) is given by a sum over all the microscopic exchange integrals weighted by the distance between spins, and is wave vector independent.[12,41] Such average will be mostly insensitive to small phase shifts in individual values of the exchange integrals

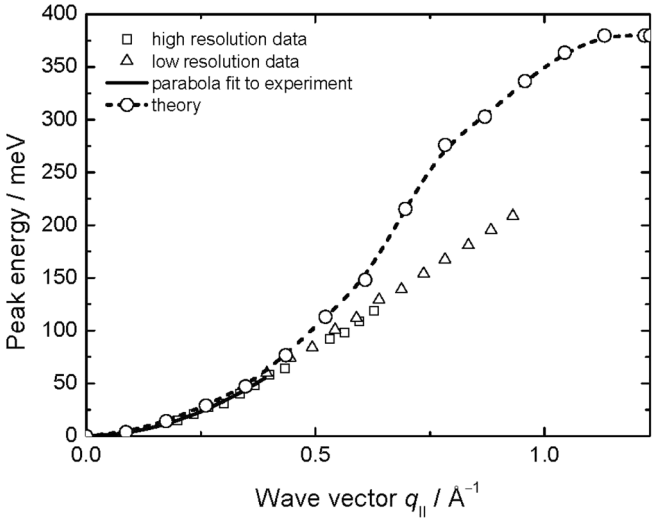

FIG. 10. Comparison of the theoretical dispersion (open circles) with experimental data (open squares and triangles).

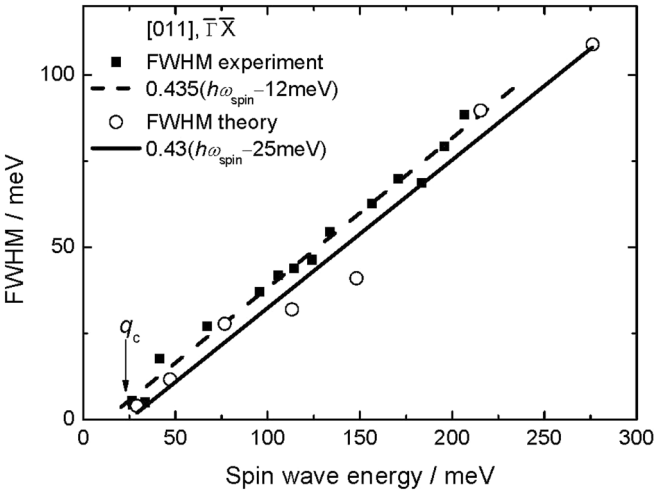

FIG. 11. Full width at half maximum (FWHM) of the spin wave peak vs the spin wave energy. Solid squares are the experimental data from Fig. 9, the open circles are from theory. When fitted to a linear relation the theoretical results follow the same slope. See text for further discussion.

due to details of the electronic structure. The large wave vector dispersion relation, however, depends on sums of products of exchange integrals by oscillatory functions of the wave vector. Small uncertainties in the determination of the electronic structure may lead to large variations of spin wave energies at large wave vectors. This may explain why the discrepancy between theory and experiment in the large wave vector region is much larger than at small wave vectors. This reasoning is especially compelling to us because the discrepancy between theory and experiment starts to increase noticeably around the same wave vector region where the dispersion relation ceases to be quadratic.

We now turn to the linewidth of the spin wave peaks. These linewidths represent the hallmark of itinerant magnetism and are a direct consequence of the system's electronic structure. No adjustable parameter was employed in their determination. We recall that the only parameters in our calculations are those describing the hopping integrals and the effective Coulomb interaction; they are the output of *ab initio* calculations specifically designed for the geometry of the system in question.

The calculated spectral linewidths agree nicely with those extracted from the experimental results for small and intermediate wave vectors. When plotted vs the spin wave energy then the agreement is nearly perfect for wave vectors up to $q_{\parallel} = 0.88$ Å, the largest wave vector for which we have attempted to deduct a FWHM from the experimental data (Fig. 11). In both cases the data are fit by a linear relation between the FWHM and the spin wave peak energy with the slope of 0.43. The only difference is a minor offset on the energy scale. This difference may be not significant, because of experimental errors in the determination of the FWHM at low energies.

The roughly linear relationship between linewidth and spin wave energy can be understood as follows: The lifetime of a spin wave with energy $\hbar\omega$ is inversely proportional to the density of Stoner excitations at $\hbar\omega$ (Landau damping), which is given by the spectral density associated with the mean-field transverse susceptibility. It has been shown[12] that this spectral density is proportional to an integral over the interval $(E_F - \hbar\omega, E_F)$ of a product of single-particle Green functions. Since $\hbar\omega$ is typically much smaller than the electronic bandwidth, the integrand is approximately constant over the integration interval and the result is roughly linear in $\hbar\omega$. According to this argument the linear relation between linewidth and energy should display zero linewidth for zero spin wave energy while the linewidth in Fig. 11 actually approaches zero for a finite spin wave energy. The reason for this is related to the spectrum of available Stoner excitations $\hbar\omega(q)$. Inspection of the band structure of fcc cobalt[42] shows that the main channel for Stoner excitations with $q_{\parallel}$ along the [110] direction closes at a minimum wave vector of $q_c = 0.25$ Å^{-1}, corresponding to a spin wave energy of 22 meV. This critical q_c is shown in Fig. 11 as an arrow pointing to the corresponding spin wave energy.

One of the main difficulties in interpreting spin wave spectra measured by electron energy loss spectroscopy comes from the very nature of the probe: The electron beam penetrates a few atomic layers close to the surface of the magnetic film and interacts in a complicated fashion with the magnetization of these layers. A complete calculation of the spectra would require detailed multiple scattering calculations combined with a spectral function that is not quite the same as the transverse susceptibility described by Eq. (18). Also details of the surface potential enter critically into such calculations since the energy of the probing electron is small.[43] Here, we merely make a crude attempt at describing the contribution of deeper layers to the calculated spin wave spectra. We assume that the electron beam penetrates the magnetic film with an exponentially decaying intensity, characterized by a decay length $\lambda_{\rm dec}$, and no phase shift. The resulting spectral density is given by

$$A_{\rm MS}(\omega) = -\frac{1}{\pi}\,{\rm Im}\sum_{l,l'} e^{-\frac{(l+l')d}{\lambda_{\rm dec}}}\,\chi^{+-}_{ll'}(\omega;\vec{q}_{||}), \qquad (20)$$

where d is the interlayer distance. The layer indices l, l' run from 0 to 7, 0 being the surface layer. The decay length

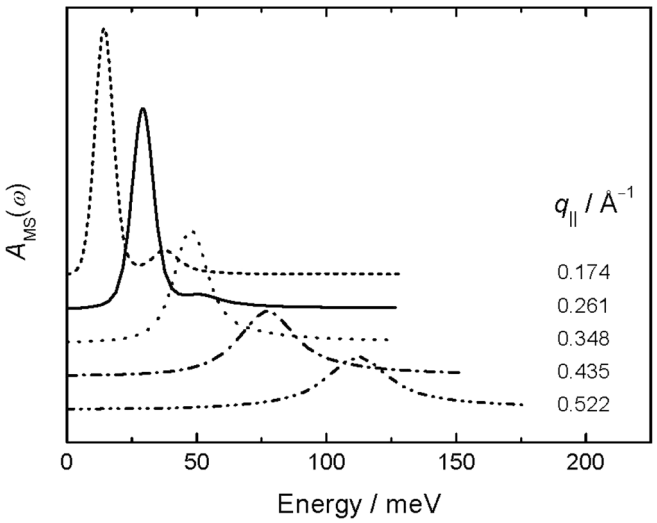

FIG. 12. Theoretical spectral densities calculated for five different wave vectors according to Eq. (20) with $\lambda = 5$ Å are shown as dashed, solid, dotted, dash-dotted, and dash-dot-dotted lines for $q_{\|} = 0.174$, 0.261, 3.48, 0.435, and 0.522 Å^{-1}, respectively. The second mode loses its character as a discernible feature at about $q_{\|} = 0.35$ Å^{-1}, in perfect agreement with experiment (Fig. 3).

λ_{dec} is estimated from the measured mean free path λ in cobalt layers. According to Vescovo *et al.*[44] the mean free path in cobalt is about 7 Å for electrons with 7 eV energy above the vacuum level (about 12 eV above the Fermi level, the reference used by Vescovo *et al.*). Given the fact that the electrons enter and leave at a mean angle of 45° we estimate λ_{dec} as $\lambda/\sqrt{2} \approx 5$ Å $\approx 2d$. We remark that the precise choice of $2d$ in the calculation is not critical. The key feature of our "poor man's multiple scattering" calculation is that more layers than just the first layer are excited by the electron beam. How much the beam actually penetrates does not change the essence of the result; it just introduces small changes in the ratio between acoustic and standing mode amplitudes.

In Fig. 12 we show $A_{MS}(\omega)$ folded with the experimental resolution for a few wave vectors along the [110] direction. For the two smallest wave vectors it is still possible to see the first standing mode as a distinguishable feature besides the main spin wave peak. At larger wave vectors there is no visible sign of the standing spin wave, although for the same wave vectors it is still visible in the spectral density projected exclusively on the surface layer (see, e.g., Fig. 1 of Ref. 14). We note that the signature of the first standing wave in the spectral densities of Fig. 12 is at variance with a recent theoretical study attempting to explain the absence of standing spin waves in previous experiments.[23] The clear sign of a second mode for wave vectors $q_{\|} = 0.174$ and 0.261 Å^{-1} in Fig. 12, as well as its absence in the spectral densities for $q_{\|} \geqslant 0.348$ Å^{-1}, is in agreement with the experimental results in Fig. 3: There, the second mode is visible in three spectra for $q_{\|}$ up to 0.3 Å^{-1} while it has merged with the now broader peak of the surface spin wave in the spectrum for $q_{\|} = 0.335$ Å^{-1} and for wave vectors beyond that value. Because of the agreement between theory and experiment we identify the experimental feature with the first standing spin wave mode of the 8-ML slab. The calculated peak energies for the standing mode lie slightly above the experimental values. This is potentially an interesting effect. Unlike the surface mode the frequency of the lowest standing wave mode depends on the number of layers and, more importantly, on the details of the interface between cobalt and copper. To the extent one is willing to believe in qualitative aspects of the Heisenberg model for this system one can show that a reduction of the effective coupling between the cobalt atoms at the interface (due to intermixing with copper, e.g.) leads to a reduction in the frequency of the standing wave mode at small $q_{\|}$. A further exploration of such effects requires a much larger experimental database and is therefore left to future studies.

VI. SUMMARY AND CONCLUDING REMARKS

By employing a recently developed electron spectrometer, surface spin waves of fcc cobalt films were studied with unprecedented energy resolution. The high-resolution spectra show standing spin wave modes which theory has predicted to exist for some time. The visibility of the standing wave mode at small wave vectors as well as their absence in larger wave vector spectra is in excellent agreement with a model based on a simplified version of a multiple scattering calculation. Since the spectrometer is completely characterized in its electron optical properties reliable data for the energy width of the surface spin waves could be obtained. We have compared our experimental data with calculations of spin wave energies and linewidths based on an *ab initio* electronic structure for the substrate and the magnetic film. Given the first-principles nature of the theory, the agreement between theory and experiment is remarkable.

ACKNOWLEDGMENTS

J.R. gratefully acknowledges financial support from NRW Research School "Forschung mit Synchrotronstrahlung in den Nano- und Biowissenschaften." A.T.C. acknowledges financial support from CNPq (Brazil). He would also like to thank Samir Lounis and Stefan Blügel for their hospitality during a one month stay at the Research Center Jülich. J.R. and H.I. acknowledge fruitful discussions with Samir Lounis.

*Deceased.

[1]R. Allenspach and A. Bischof, Phys. Rev. Lett. **69**, 3385 (1992); F. Baudelet, M.-T. Lin, W. Kuch, K. Meinel, B. Choi, C. M. Schneider, and J. Kirschner, Phys. Rev. B **51**, 12563 (1995).

[2]N. Weber, K. Wagner, H. J. Elmers, J. Hauschild, and U. Gradmann, Phys. Rev. B **55**, 14121 (1997); A. Kubetzka, P. Ferriani, M. Bode, S. Heinze, G. Bihlmayer, K. von Bergmann, O. Pietzsch, S. Blügel, and R. Wiesendanger, Phys. Rev. Lett. **94**, 087204 (2005).

[3]M. Bode, M. Heide, K. von Bergmann, P. Ferriani, S. Heinze, G. Bihlmayer, A. Kubetzka, O. Pietzsch, S. Blügel, and R. Wiesendanger, Nature **447**, 190 (2007); S. Heinze, K. von Bergmann, M. Menzel, J. Brede, A. Kubetzka, R. Wiesendanger, G. Bihlmayer, and S. Blügel, Nat. Phys. **7**, 713 (2011).

[4]H. Ibach, D. Bruchmann, R. Vollmer, M. Etzkorn, P. S. Anil Kumar, and J. Kirschner, Rev. Sci. Instrum. **74**, 4089 (2003).
[5]H. Ibach, J. Rajeswari, and C. M. Schneider, Rev. Sci. Instrum. **82**, 123904 (2011).
[6]R. Vollmer, M. Etzkorn, P. S. Anil Kumar, H. Ibach, and J. Kirschner, Phys. Rev. Lett. **91**, 147201 (2003).
[7]M. Etzkorn, P. S. Anil Kumar, R. Vollmer, H. Ibach, and J. Kirschner, Surf. Sci. **566–568**, 241 (2004).
[8]W. X. Tang, Y. Zhang, I. Tudosa, J. Prokop, M. Etzkorn, and J. Kirschner, Phys. Rev. Lett. **99**, 087202 (2007); J. Prokop, W. X. Tang, Y. Zhang, I. Tudosa, T. R. F. Peixoto, Kh. Zakeri, and J. Kirschner, *ibid.* **102**, 177206 (2009).
[9]Kh. Zakeri, Y. Zhang, J. Prokop, T. H. Chaung, N. Sakr, W. X. Tang, and J. Kirschner, Phys. Rev. Lett. **104**, 137203 (2010).
[10]Y. Zhang, P. Buczek, L. Sandratskii, W. X. Tang, J. Prokop, I. Tudosa, T. R. F. Peixoto, Kh. Zakeri, and J. Kirschner, Phys. Rev. B **81**, 094438 (2010).
[11]Y. Zhang, P. A. Ignatiev, J. Prokop, I. Tudosa, T. R. F. Peixoto, W. X. Tang, Kh. Zakeri, V. S. Stepanyuk, and J. Kirschner, Phys. Rev. Lett. **106**, 127201 (2011).
[12]R. B. Muniz and D. L. Mills, Phys. Rev. B **66**, 174417 (2002).
[13]R. B. Muniz, A. T. Costa, and D. L. Mills, J. Phys.: Condens. Matter **15**, 495 (2003).
[14]A. T. Costa, R. B. Muniz, and D. L. Mills, Phys. Rev. B **69**, 064413 (2004).
[15]A. T. Costa, R. B. Muniz, and D. L. Mills, Phys. Rev. B **70**, 054406 (2004).
[16]H. A. Mook and D.McK. Paul, Phys. Rev. Lett. **54**, 227 (1985).
[17]M. Etzkorn, P. S. Anil Kumar, W. Tang, Y. Zhang, and J. Kirschner, Phys. Rev. B **72**, 184420 (2005).
[18]M. Etzkorn, Thesis, Martin-Luther University Halle-Wittenberg, urn:nbnde:gbv:3-000008590, 2005.
[19]H. Ibach and J. Rajeswari, J. Electron Spectrosc. Relat. Phenom. **185**, 61 (2012).
[20]C. L. Gao, A. Ernst, G. Fischer, W. Hergert, P. Bruno, W. Wulfhekel, and J. Kirschner, Phys. Rev. Lett. **101**, 167201 (2008).
[21]M. P. Gokhale, A. Ormeci, and D. L. Mills, Phys. Rev. B **46**, 8978 (1992); H. Tang, M. Plihal, and D. L. Mills, J. Magn. Magn. Mater. **187**, 23 (1998).
[22]A. T. Costa, R. B. Muniz, and D. L. Mills, Phys. Rev. B **68**, 224435 (2003).
[23]A. Taroni, A. Bergman, L. Bergqvist, J. Hellsvik, and O. Eriksson, Phys. Rev. Lett. **107**, 037202 (2011).
[24]C. M. Schneider, P. Bressler, P. Schuster, J. Kirschner, J. J. de Miguel, and R. Miranda, Phys. Rev. Lett. **64**, 1059 (1990); C. M. Schneider, P. Bressler, P. Schuster, J. Kirschner, J. J. de Miguel, R. Miranda, and S. Ferrer, Vacuum **41**, 503 (1990).
[25]F. Huang, M. T. Kief, G. J. Mankey, and R. F. Willis, Phys. Rev. B **49**, 3962 (1994).
[26]T. Allmers and M. Donath, Surf. Sci. **605**, 1875 (2011).
[27]H. Ibach, M. Etzkorn, and J. Kirschner, Surf. Interface Anal. **38**, 1615 (2006).
[28]T. Duden and E. Bauer, Proc. Mater. Res. Soc. **475**, 283 (1997).
[29]H. Ibach and D. L. Mills, *Electron Energy Loss Spectroscopy and Surface Vibrations*. (Academic Press, New York, 1982).
[30]Lord Rayleigh, Proc. London Math. Soc. **17**, 4 (1887).
[31]M. H. Mohamed, J.-S. Kim, and L. L. Kesmodel, Surf. Sci. **220**, L687 (1989).
[32]W. Daum, C. Stuhlmann, and H. Ibach, Phys. Rev. Lett. **60**, 2741 (1988).
[33]A. Taylor and Brenda J. Kagle, *Crystallographic Data on Metal and Alloy Structures*. (Dover Publications, New York, 1963).
[34]X. Liu, M. M. Steiner, R. Sooryakumar, G. A. Prinz, R. F. C. Farrow, and G. Harp, Phys. Rev. B **53**, 12166 (1996).
[35]W. Feller, *An Introduction to Probability Theory and Its Applications*, 3rd ed. (Wiley, New York, 1968).
[36]S. Lounis, A. T. Costa, R. B. Muniz, and D. L. Mills, Phys. Rev. B **83**, 035109 (2011).
[37]A. T. Costa, R. B. Muniz, S. Lounis, A. B. Klautau, and D. L. Mills, Phys. Rev. B **82**, 014428 (2010).
[38]P. R. Peduto, S. Frota-Pessa, and M. S. Methfessel, Phys. Rev. B **44**, 13283 (1991); Sonia Frota-Pessoa, *ibid.* **46**, 14570 (1992); O. K. Andersen, *ibid.* **12**, 3060 (1975); O. K. Andersen, O. Jepsen, and D. Glötzel, in *Highlights in Condensed Matter Theory*, edited by F. Bassani, F. Fumi, and M. P. Tosi (North Holland, Amsterdam, 1985).
[39]R. Haydock, in *Solid State Physics*, edited by H. Ehrenreich, F. Seitz, and D. Turnbull (Academic Press, New York, 1980), Vol. 35.
[40]U. von Barth and L. A. Hedin, J. Phys. C **5**, 1629 (1972).
[41]D. M. Edwards and R. B. Muniz, J. Phys. F **15**, 2339 (1985).
[42]C. M. Schneider, P. Schuster, M. Hammond, H. Ebert, J. Noffke, and J. Kirschner, J. Phys.: Condens. Matter **3**, 4349 (1991).
[43]B. M. Hall, S. Y. Tong, and D. L. Mills, Phys. Rev. Lett. **50**, 1277 (1983).
[44]E. Vescovo, C. Carbone, U. Alkemper, O. Rader, T. Kachel, W. Gudat, and W. Eberhardt, Phys. Rev. B **52**, 13497 (1995).